ENSO Bred Vectors in Coupled Ocean–Atmosphere General Circulation Models

S.-C. YANG,* M. CAI,+ E. KALNAY,* M. RIENECKER,# G. YUAN,@ AND Z. TOTH&

*Department of Meteorology, University of Maryland, College Park, College Park, Maryland
+Department of Meteorology, The Florida State University, Tallahassee, Florida
#Global Modeling and Assimilation Office, NASA GSFC, Greenbelt, Maryland
@Bauer Center for Genomics Research, Harvard University, Cambridge, Massachusetts
&Environmental Modeling Center, NOAA/National Centers for Environmental Prediction, Camp Springs, Maryland

(Manuscript received 12 October 2004, in final form 13 September 2005)

ABSTRACT

The breeding method has been implemented in the NASA Seasonal-to-Interannual Prediction Project (NSIPP) coupled general circulation model (CGCM) with the ultimate goal of improving operational seasonal to interannual climate predictions through ensemble forecasting and data assimilation. This is the first attempt to isolate the evolving ENSO instability and its corresponding global atmospheric response in a fully coupled ocean–atmosphere GCM. The results herein show that the growth rate of the coupled bred vectors (BVs) is sensitive to the ENSO phases of the evolving background flow and peaks about 3 months before an ENSO event. The structure of the dominant growing BV modes also evolves with the background ENSO and exhibits a larger amplitude in the eastern tropical Pacific, reflecting the natural dynamical sensitivity associated with the shallow thermocline at the eastern boundary. The key features of coupled bred vectors of the NSIPP CGCM are reproduced when using the NCEP CGCM, an independently developed coupled general circulation model.

Introduction

The El Niño–Southern Oscillation (ENSO) phenom-on is responsible for a large portion of interannual riability in the tropical Pacific. ENSO also has a glob-impact in climate anomalies and extreme weather ents. Feedbacks through atmosphere–ocean coupling the Tropics characterize the covariability of wind, T, and thermocline (or warm water volume) of NSO. Many features of the ENSO events have been plained by the delayed oscillator mechanism owing to opagating downwelling/upwelling information in the per ocean associated with equatorial waves (Schopf d Suarez 1988; Suarez and Schopf 1988; Battisti 88). Jin (1997) further emphasized the importance of variations of warm water volume in the upper ocean th a warm water recharge/discharge mechanism. It s been shown that the coupled dynamic/thermody-mic mechanisms, that is, the thermocline and Ekman dbacks, responsible for delayed or recharge/discharge oscillators, can explain both the west–east asymmetry in the climate mean state and the ENSO variability in the equatorial Pacific basin (Cai 1995; Jin 1996; Dijkstra and Neelin 1999; Van der Vaart et al. 2000; Cai 2003). The dynamical atmosphere–ocean coupled models constructed with the concept of the delayed or recharge/discharge oscillator have shown valuable prediction skill for the ENSO events (Cane et al. 1986; Zebiak and Cane 1987). The strong weather and climate impact from ENSO has motivated the advancement of prediction tools from simple anomaly coupled models to fully coupled global ocean–atmosphere general circulation models (CGCMs).

Factors that influence the skill in forecasting seasonal–interannual SST anomalies include the errors in oceanic and atmospheric initial conditions, atmospheric stochastic variability, and model errors. It is known that the presence of errors in the initial condition limits the ENSO prediction skill (Latif et al. 1998) and that an ensemble forecast should sample the uncertainties in the initial condition (Stockdale et al. 1998). Vialard et al. (2003) performed a series of ensemble forecast experiments with a state-of-the-art coupled GCM using wind and SST perturbations and stochastic physics, in-

Corresponding author address: Dr. Ming Cai, Department of teorology, The Florida State University, Tallahassee, FL 06.

hat the uncertainties in SST determine the spread semble forecasts in early months of the forecast, perturbations of the wind stress or atmospheric al variability are less efficient in generating SST ions. These results are supported by Chen et al.) who argue that the evolution of El Niño is cond to a large degree by self-sustaining internal dys in the Tropics. These results suggest that the D prediction depends more on initial conditions on unpredictable atmospheric noise and that there ood reason to investigate the inclusion of coupled perturbations for ensemble ENSO prediction.

the ENSO ensemble prediction, the challenge is o generate ensemble perturbations that can effec- represent SST uncertainties in seasonal–interancale in a CGCM. Moreover, initial ensemble pertions need to be constructed in a coupled manner der to ensure that they reflect the uncertainties ated with the coupled instability. In addition, ene perturbations for ENSO prediction should also t the uncertainties in teleconnected atmospheric bles to improve coupled forecast skill beyond the al Pacific region.

thods for generating ensemble perturbations can osely categorized into linear and nonlinear aphes. The singular vector linear approach looks for ptimal initial perturbations that will maximize the h of the perturbations after a chosen period with osen norm. With an optimization time of 3–6 hs and the choice of the SST norm, Penland and shmukh (1995), Chen et al. (1997), and Thomp998) showed that a final singular vector with large tude of the SST signal is located in the southeastacific. It should be pointed out that, even though rowth rate of their singular vector strongly de- on seasonal cycle and ENSO phase, their initial ar vectors are *insensitive to both*. However, also a SST norm, Xue et al. (1994, 1997a,b) and Fan et 000) obtained ENSO-like initial singular vectors, asizing that the signals in the eastern Pacific are concentrated toward the equator, even though final singular vectors are very similar to those in Chen et al. (1997) and Thompson (1998). Fi- a very different pattern compared to all of the studies has been obtained from a series of studies by Moore and Kleeman (1996, 1997, 1999a,b, . Their results emphasize large signals in the west ntral Pacific. When considering a multivariable rbation norm, Fan et al. (2000) and Moore and man (2001) reached different conclusions on the ve importance between the SST and the therne. The strong dependence on the choice of norm conclusion as to their use for ENSO ensemble perturbations. Moreover, with a very complex system like a CGCM that includes a wide range of instabilities, leading singular vectors would be dominated by the fast growing error related to weather and even convection (Peña and Kalnay 2004). Thus, to obtain an ENSO-related singular vector in a coupled GCM, one needs to exclude less relevant fast growing components explicitly from the tangent linear operator (Kleeman et al. 2003). The computational/development costs are also a limitation for the singular vector method since it requires constructing coupled tangent linear and adjoint operators.

The breeding method proposed by Toth and Kalnay (1993, 1997) is designed to estimate the shape of the growing dynamic error using the full nonlinear model. This method takes advantage of the early nonlinear saturation of convective instabilities compared to baroclinic instabilities. Toth and Kalnay (1996) suggested this advantage could be applied in a coupled ocean–atmosphere system to isolate ENSO coupled instabilities from the faster weather-related instabilities. Cai et al. (2003) first tested the breeding method in a coupled system using the ZC model (Zebiak and Cane 1987). They found that the bred vector (BV) growth rate is weakest at the peak time of the ENSO states (both positive and negative) and strongest between the events. Also, the coupled bred vectors are insensitive to the choice of norm but very sensitive to the background ENSO phase and the annual cycle. It should be pointed out that the ZC model only has ENSO-related instability and the fast processes are already explicitly excluded from the ZC model. Peña and Kalnay (2004) illustrated the idea that breeding is able to isolate the slow modes of a coupled system when rescaling intervals and amplitudes are chosen from physically appropriate scales and the rescaling factor is obtained from the slow component of the system. Independent work by Boffetta et al. (1998) also demonstrated that choosing the perturbation size is a powerful tool to isolate the slow mode in a system with multiple time scales.

The results with the simple ZC model encouraged us to implement the breeding method in a CGCM, without sacrificing resolution or simplifying model physics. The new challenge is that a CGCM includes many types of instabilities with different time scales. Therefore, we need to demonstrate, as a first step, whether we can obtain the slowly growing coupled instabilities as in Cai et al. (2003) using breeding in a comprehensive CGCM. Our objective is to identify the characteristics of bred vectors associated with the ENSO derived from the CGCM and to investigate whether an ENSO-related tabilities using the breeding method. Specifically, in s paper, we address the following questions. 1) Can eeding be used to identify or detect the coupled, wly growing ENSO instability and isolate it from her short-term instabilities? 2) Is the coupled BV de sensitive to the ENSO phases? and 3) Are the in characteristics of coupled bred vectors reproduc- e with different coupled ocean–atmosphere GCMs?

The paper is organized as follows. In section 2, we e a brief description of the National Aeronautics and ace Administration's (NASA's) Seasonal-to- erannual Prediction Project (NSIPP) coupled model t has been used to generate coupled bred vectors. e simulated ENSO variability in the NSIPP model is o included in section 2. Section 3 describes how the eeding method is applied in a coupled GCM for iso- ing the slowly varying coupled instability. Section 4 scribes the main characteristics of coupled bred vec- s derived in the NSIPP model. A comparison of the ults obtained from NSIPP and from the National nters for Environmental Prediction Coupled Fore- t System Model (NCEP/CFS03) is also presented in tion 4. A brief summary and discussion of the next ase of our research are included in section 5.

Breeding method with the NSIPP coupled global circulation model

n this study, we implemented the breeding method the NSIPP coupled ocean–atmosphere general cir- ation model. The NSIPP coupled model is a fully upled global ocean–atmosphere–land system devel- ed at the NASA Goddard Space Flight Center SFC) (Vintzileos et al. 2003). It comprises the NSIPP mospheric model (AGCM) (Bacmeister and Suarez 02; Bacmeister et al. 2000), the Poseidon ocean del (OGCM) (Schopf and Loughe 1995; Yang et al. 99), and the Mosaic land surface model (LSM) (Ko- r and Suarez 1992). The official NSIPP Web site ntains detailed information about the NSIPP coupled del (http://nsipp.gsfc.nasa.gov/).

A 62-yr simulation run had been made with a re- rch version of the NSIPP CGCM with a resolution 3° latitude by 3.75° longitude and 34 sigma layers in e AGCM and ½° latitude by 1.25° longitude and 27 ers in the OGCM. This integration constitutes our ature run" and is referred to as the "background" in s paper. The bred perturbations are grown upon the olving background flow. The wind stress, SST, and ermocline anomalies from this long simulation ex- it coupled ENSO interannual variability. However, e ENSO cycle of the control run has an unrealistically ong biennial component rather than the observed

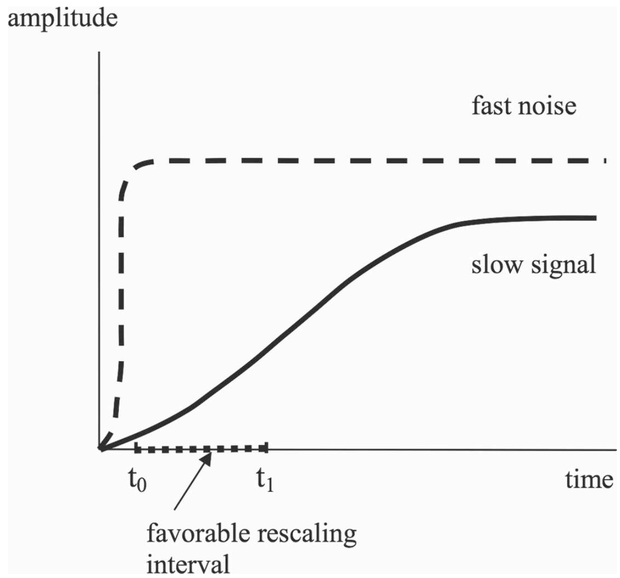

FIG. 1. Schematic showing that, if the rescaling time interval for breeding is larger than t_0, the saturation time of the fast noise, and smaller than the time t_1, when nonlinearities reduce the growth of the slow signal, the relative amplitude of the linearly growing slow signal is boosted with respect to the noise.

viation of the SST anomaly in the eastern Pacific is only half of the observed. This problem has been attributed to the atmospheric longitudinal circulation near the equator (Rienecker et al. 2000). The spatial patterns of the coupled ENSO variability of the background are shown in the left panels of Figs. 4–6 and will be discussed together with the bred vector spatial structure in section 3.

We used a 10-yr model simulation run to perform breeding experiments under a "perfect model scenario," that is, assuming that the unperturbed simulation run is the "truth" (or analysis in a forecast system). The breeding method (Toth and Kalnay 1993, 1996, 1997) was originally developed to "breed" growing modes related to synoptic baroclinic instability for short-to-medium range atmospheric ensemble forecasting by taking advantage of the fact that small amplitude, but faster growing, convective instabilities saturate earlier. The idea that different amplitudes and time scales characterize different types of instabilities is applied to isolate the slowly growing coupled ENSO instability from the fast growing weather signal (see schematic Fig. 1). This is difficult to do using atmospheric variables since the amplitude of the weather noise is larger than that of the ENSO-related coupled signal. The slow, coupled perturbation can only be isolated by measuring the growing perturbations using the slowly evolving component of the coupled system, namely the

the period longer than two weeks is important in to estimate the slowly varying coupled instability aturate the growth of the weather signal (Peña and y 2004).

e procedure of breeding cycles in a coupled system een described in Cai et al. (2003). Bred vectors are eriodically rescaled difference between the perd run and the nonperturbed run (background). escaling period (longer than two weeks) is chosen ow fast weather instabilities to saturate well before escaling time, whereas the slowly evolving ENSO bility is still growing (Fig. 1). Both oceanic and spheric perturbations are scaled down with the factor, measured by the growth of the ocean comnt. This gives a relative advantage to the slowly ng ENSO mode (as well as to any other slow inty present in the coupled system). In the next ing cycle, the saturated fast instability perturbatarts with an unfavorable shape and does not have room to grow, but the slow ENSO instability from a favorable (linear) shape that can still grow volve. Therefore, by repeating the breeding proe (periodically resizing the perturbation and addto the background) we can enhance the relative tude of the slow instability and allow the bred rbation to align along favorable growing direc- Although this does not completely isolate the) perturbation, it gives it a relative boost com- to faster growing perturbations that saturate 1), but other instabilities with time scales longer he weather instabilities will be also present in the n the next section, we focus on the dynamic strucf the coupled bred vector associated with the evo- of the background, which is viewed as "nature" erfect model scenario, since in this study we are oncerned with model error.

e breeding method was implemented in the NSIPP M with a 1-month rescaling period and using the ifference in the Niño-3 SST within the tropical c domain (15°S–15°N, 120°E–90°W) as the rescalorm. The rescaling amplitude of the rms SST was n to be 0.085°C, or about 10% of the background ariability. The 1-month rescaling period, which is longer than the time scale of the atmospheric linic instability, is also a convenient choice be- in the NSIPP system users can access only nly model output. According to the experience in al. (2003) with the ZC model, the structure of the vector is rather insensitive to either the choice of scaling period (if it is long enough to saturate the er signal) or the choice of the slow variable norm r the oceanic energy norm). Also, breeding experiments with the NCEP coupled GCM using 15 days as the rescaling period have a similar behavior of the BV growth rate as with a 1-month rescaling period. The rescaling norm must be associated with the ocean component in order to capture the slowly growing instability. Since the SST directly represents the strength of the ENSO variability, it is natural to use it to detect the growing coupled instability. Because the research version of the NSIPP coupled GCM used in this paper is no longer available, it was not possible to test different breeding rescaling norms. However, tests with the operational version of the NSIPP coupled GCM show that the BV structure obtained is robust when using either a SST norm measured in the Niño-3 region or a thermocline norm measured in the tropical Pacific.

Two independent breeding runs were made starting from two perturbations created by taking the difference between two model states at randomly chosen months. Each run contains 123 months, starting from September of the 19th year to December of the 29th year of the 62-yr simulation run. The starting month is chosen to be well separated from the first major warming event, which takes place about 2 years into the breeding run. This is to ensure that the breeding experiment does not start when the background is dominated by the mature ENSO condition. Two independently generated breeding experiments show that bred vectors start to have similar structure after three months. Thus, we treat the first three months as a transient period allowing the bred vectors to align along the dynamics-dominated instability. The analysis presented below is derived from the remaining 120 breeding cycles (120 months). We found that two independent 10-yr breeding cycles yielded very similar bred vectors (not shown), so we combine the two bred vector perturbations as a single time series of 20 years to reduce sampling errors. Hereafter, we refer to the combined bred vectors as BV perturbations.

3. Results

a. Growth rate of coupled bred vectors

Bred vectors represent, by construction, the instabilities that have been growing in the recent past upon the background flow. In addition to ENSO, our method captures any instability with a time scale longer than 2 weeks. An example of such instability is shown in Fig. 2, a snapshot of the bred vector SST field (contours) together with the corresponding background SST field (shading) on 1 July of model year 24. It shows that the bred vector field has a large amplitude along the sharp zonal temperature gradient in the equatorial cold tongue, where tropical instability waves are present in

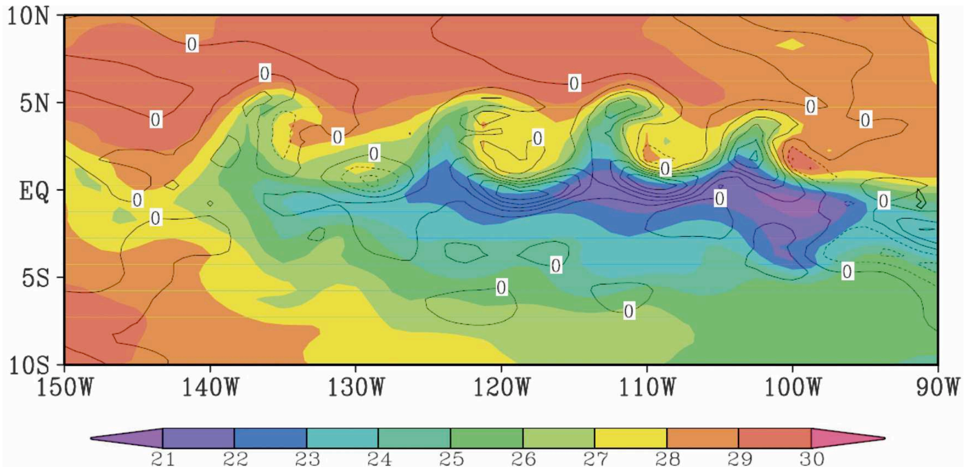

FIG. 2. A snapshot of SST in the eastern Pacific showing the bred vectors' perturbation (contours: CI = 0.15°C) evolving with the background flow (shading with an interval of 1°C from 21° to 30°C) on 1 July of model year 24. The dotted contours of the BV indicate negative values.

ed perturbation is aligned with the background flow such a way as to increase the amplitude of the waves. opical wave instability is active when the cold tongue well established, like the fall season and the La Niña ents, in both the background and the BV fields. The t that the bred vector can capture the formation of pical instability waves suggests BV sensitivity to the olution of the background flow since the formation of ch instability is strongly influenced by seasonal and erannual variability (Contreras 2002). We found that BV structures related to the tropical instability ves disappear when the background is evolving tord a warm anomalous state. This example indicates t we can view the growth of the perturbations as a ult of the superposition and competition among inbilities with different physical mechanisms and time les. To analyze the ENSO component among all owth signals, we examine the relationship between BV growth rate and the background ENSO varility, described by the Niño-3 index.

The growth rate of the coupled bred vectors is calated based on the chosen rescaling norm of the perbation field within the tropical Pacific region:

$$G(t) = \frac{\sqrt{\sum_{\mathrm{NG}} [\mathrm{BV}_{\mathrm{SST}}(t)]^2}}{\sqrt{\sum_{\mathrm{NG}} [\mathrm{BV}_{\mathrm{SST}}(t-1)]^2}}, \tag{1}$$

ere NG is the total number of model grid points in Niño-3 region and t is the model time in months. In her words, we measure the growth rate of bred vecs by their amplification factor in the Niño-3 region hin a month. In the 10-yr experiment, the mean of deviation is 0.7. The mean growth rate is much higher than the result obtained from Cai et al. (2003), which has an ENSO growth rate ranging between 1 and 3. This is to be expected since the presence of additional instabilities in the coupled GCM contributes to the total growth of the perturbations, compared to the ZC model. For example, the tropical wave instability shown in Fig. 2 grows vigorously but with a shorter time scale than the ENSO variability.

To test whether there is a component of the perturbation growth (above the background noisy growth rate of about 3 per month) evolving upon the coupled ENSO background state (rather than growing randomly), we calculate the lag/lead correlation between the growth rate and the absolute value of the background Niño-3 index. We use the absolute value of the Niño-3 index in order to account for the large amplitude of both positive and negative SST anomalies. It is evident in Fig. 3 that the growth rate of coupled bred vectors tends to be largest about 3–4 months prior to the time when the background ENSO amplitude reaches its maximum stage (positive or negative).

Since the coupled GCM contains different types of instabilities, the correlation level of 0.22 in Fig. 3, although small, is significant in the context of the relative amplitude of the ENSO variability. To test statistical significance, we constructed the correlation between 1000 randomly generated time series and the absolute value of the background Niño-3 index. Each time series has the same mean and variance as the time series of the bred vector growth rates. Among the 1000 random samples, the mean correlation value is 0.017 and the standard deviation is 0.07. The accumulated percentage

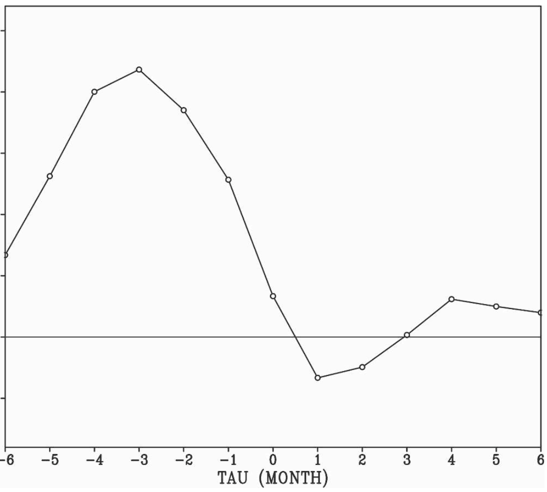

3. Lead/lag correlations between the BV growth rate and the absolute value of the background Niño-3 index.

level is close to 99% in stating that a 0.2 corre- value represents a significant correlation to the round Niño-3 index. Therefore, the maximum in 3 supports the conclusion that the bred vector h rate is related to and leads the background 3 index.

addition, the main growth signal takes place be- he ENSO events in Fig. 3 because, by taking the ute value of the background ENSO index in com- g the correlation we consider the ENSO phases and treat the cold and the warm cases as if they the same. In Cai et al. (2003), the available time was much longer so that the background Niño-3 for the ZC model was composited over many and the results arranged evolving from the cold to the warm stage. This resulted in the peak of the vector growth rate split equally before and after NSO event. We can conclude that our results are atively in good agreement with those obtained the ZC model in Cai et al. (2003). The results n here suggest that the breeding method can serve ect the slow, coupled instability related to ENSO bility by selecting the proper rescaling parameter breeding cycle. Evans et al. (2004) also showed he bred vector growth rate could be used to detect rthcoming regime changes of the background state positive to negative conditions or vice versa).

e structure of the coupled BV mode

e spatial patterns of the ENSO coupled BV ng all the instabilities present in the system) can entified by constructing regression maps for both ic and atmospheric variables against the BV SST in the Niño-3 domain. Such spatial structure of the bred vector indicates the linear response related to the ENSO instability and makes the low-frequency variations associated with ENSO clearer. We will compare the ENSO BV maps with the background ENSO regression maps constructed with the same regression method but using the background Niño-3 index. This will allow us to assess whether the coupled BV has a dominant ENSO growing component, whether it projects on the background ENSO variability, and what physical mechanisms are suggested by the BV ENSO patterns.

The oceanic global regression maps for the background fields show typical tropical variability corresponding to the ENSO mature stage (Figs. 4a–c). These patterns include a large warming extending from the east to central equatorial Pacific, a deepening thermocline in the eastern equatorial Pacific, an accompanying shoaling feature off the equator in the western basin, and a basinwide eastward current anomaly. The regression maps for the BV fields (regressed upon the BV Niño-3 index) are shown in Figs. 4d–f. The coupled BV mode exhibits a strong signal in the equatorial Pacific and fairly weak variability away from the Tropics. The patterns of the coupled BV mode are reminiscent of those in the background state except that the BV mode is more confined to the east and to the equator. This feature is physically meaningful since it reflects that the dynamical growing perturbation is mainly determined by the background structure of the thermocline. It is also consistent with the delayed oscillator theory, which considers that the perturbations grow primarily over the eastern equatorial basin through the proportionality between wind stress and the displacement of the thermocline (Cane et al. 1990). The shoaling thermocline in the east implies that the thermodynamic feedback between SST and near-surface ocean variables is much stronger in the east than in the west. As a result, oceanic perturbations in the eastern basin will be easily amplified through positive feedbacks from air–sea interaction. Although we have obtained the ENSO BV by regression with the BV Niño-3 index, Figs. 4d–f can also be referred to as the leading BV mode because they have the same structure as the leading mode obtained by applying EOF analysis to the oceanic BV (as shown in Figs. 8a,b).

The atmospheric components of the ENSO mode derived from both the background and the BV field are displayed in Fig. 5. In the same way that the background regression maps shown in Figs. 5a–d reflect the typical atmospheric response of ENSO events, the BV atmospheric regression map also exhibits the coupled feature corresponding to the boundary heating pertur-

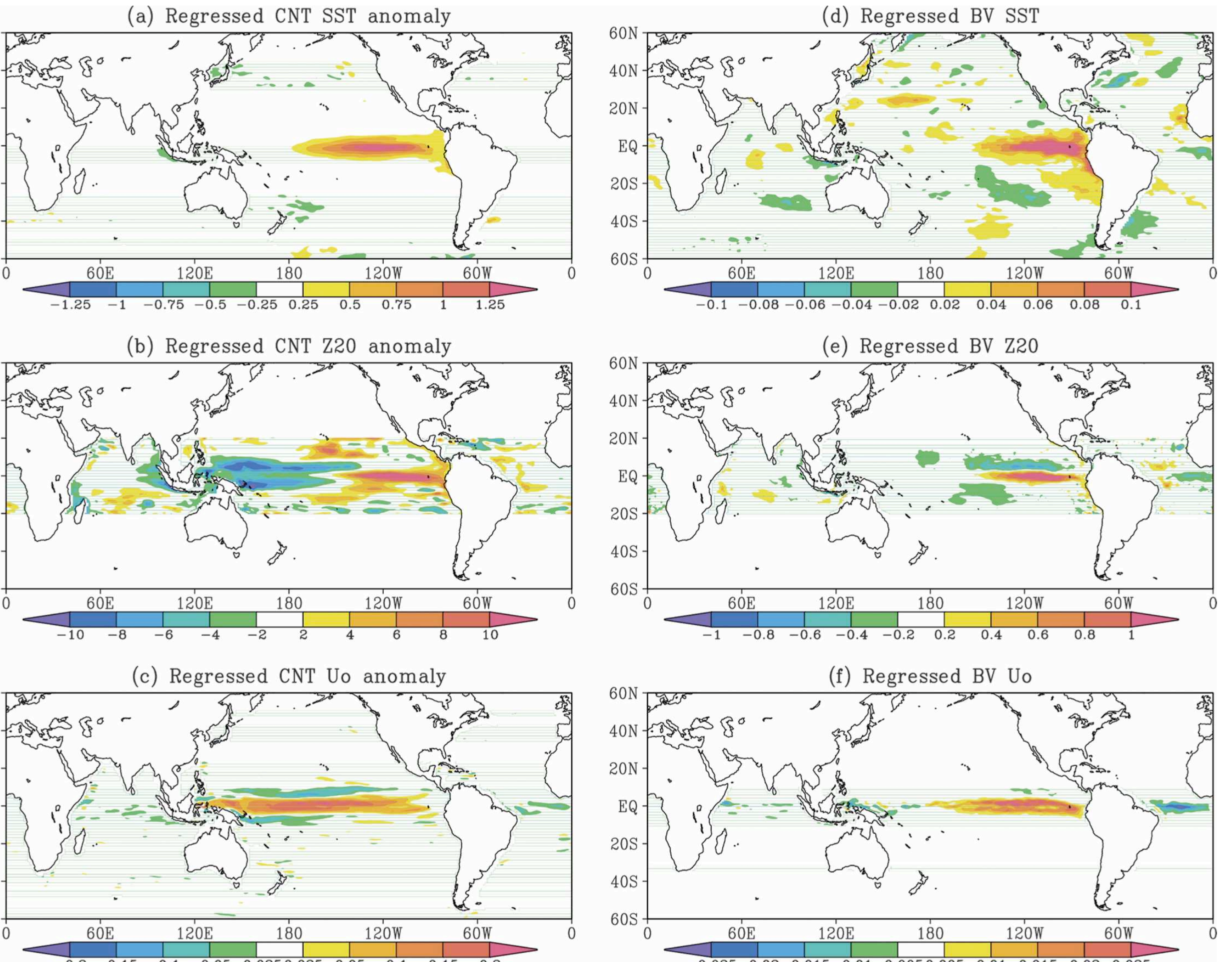

IG. 4. Oceanic regression maps in the global domain: (left) the background fields and (right) the BV fields. (a) SST anomaly (°C); Z_{20} anomaly (m); (c) surface zonal current anomaly (m s^{-1}); (d) BV SST (°C); (e) BV Z_{20} (m); and (f) BV surface zonal current s^{-1}). Background fields are regressed with the background Niño-3 index and BV fields are regressed with the BV Niño-3 index. The les of BV fields are arbitrary, but the ratio among BV variables (both oceanic and atmospheric variables) is retained as in the ginal. The background Z_{20} anomaly and BV Z_{20} are only plotted within 20°N/S, since Z_{20} is defined as the depth of the 20° isotherm, t is not well defined beyond the Tropics.

ns in the BV fields have some features in common h the patterns of the background state, such as the sterly wind perturbations located in the central equa- ial Pacific and the high–low pattern in the BV sur- e pressure field. The baroclinic structure in the ght fields corresponds to the location of BV SST in . 4d. In addition, the BV outgoing radiation reflects enhanced convection activity in the eastern basin. is atmospheric structure, implying that an amplified turbation in the eastern Pacific induces a westerly nal wind perturbation, indicates unstable air–sea in- action in the eastern Pacific. These features suggest t the bred perturbation is related to the coupled tability and therefore that we can refer it to as the upled BV mode.

present in coupled GCMs, that is, the simulated SST variability in the eastern Pacific is smaller than the observed variability. Rienecker et al. (2000) suggest that such deficiencies may be associated with the atmospheric circulation in the tropical eastern Pacific not representing well the Walker circulation, which also limits the spread of ensemble SSTs. The high–low pressure patterns in Figs. 5f,g suggest that the coupled BV is able to reflect the impact of coupled instability upon the background atmospheric circulation by perturbing the longitudinal Walker circulation along the equator.

It is of interest to point out that the coupled BV also reflects the sensitivities in extratropical regions associated with background ENSO atmospheric teleconnections. Shown in Fig. 6 are the regression maps of surface

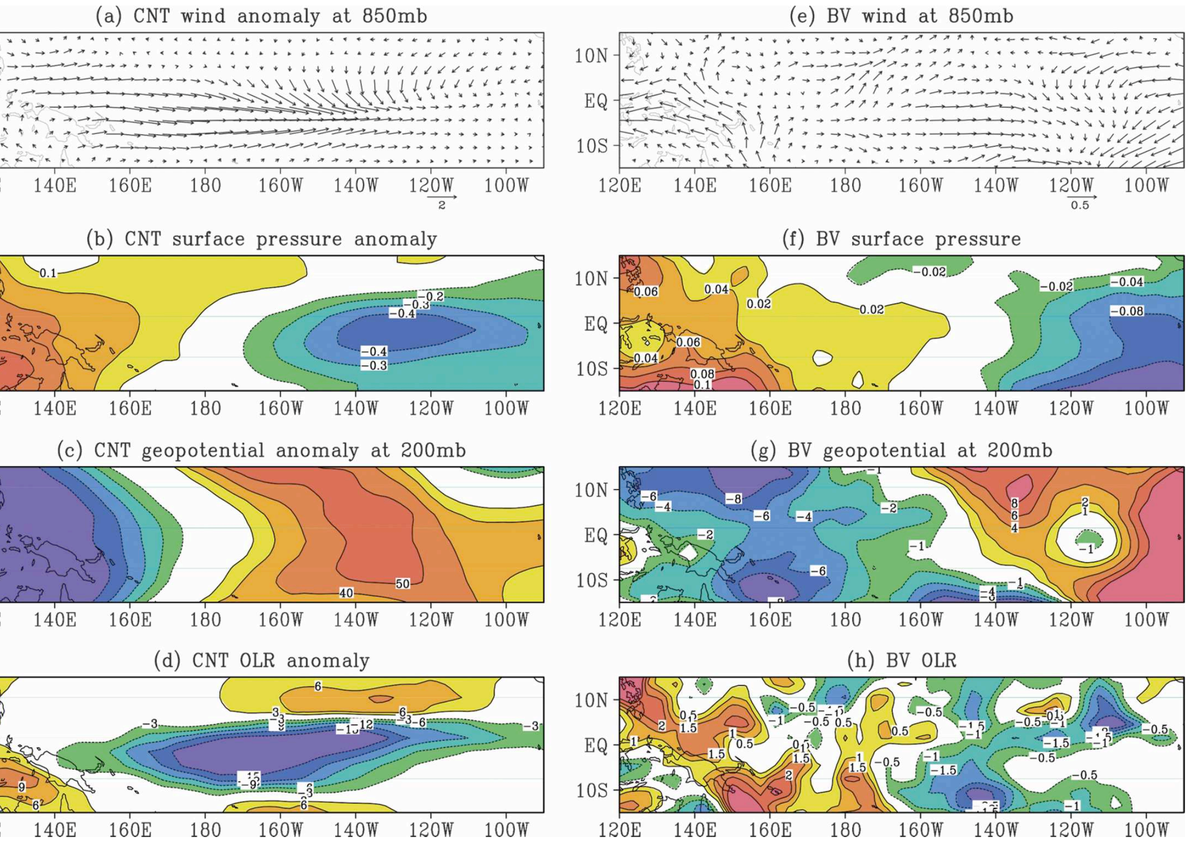

5. As in Fig. 3 except for the atmospheric regression maps over the equatorial Pacific basin: (a) wind field anomaly at 850 hPa); (b) surface pressure anomaly (hPa); (c) geopotential anomaly at 200 hPa ($m^2\ s^{-2}$); (d) outgoing longwave radiation (W m^{-2}); wind field at 850 hPa (m s^{-1}); (f) BV surface pressure (hPa); (g) BV geopotential at 200 hPa ($m^2\ s^{-2}$); and (h) BV outgoing ve radiation (W m^{-2}).

sphere for the background state and for the BV The teleconnection patterns of the background indicate a low pressure anomaly over the North c and a high pressure anomaly over North ica. This teleconnection pattern has a barotropic ure that extends from the surface to 100 hPa. It is ed by wave train patterns associated with the scale heating in the Tropics. Strong responses can e identified in those regions in the BV maps, ially where background regression maps show a g gradient, for example in the mid-Pacific at 30°N t east coast of North America. Wave train pat-can also be found in BV regression maps. In the ern extratropical region (not shown), atmospheric ssion maps also have a teleconnected pattern as-ed with the background ENSO, and we observe d BV dynamical sensitivities.

show the sensitivity of the coupled BV mode to ackground ENSO evolution, we construct nth lead/lag correlation maps against the time se-f the amplitude of the background Niño-3 index using the first 10 EOF modes to illustrate the dominant signals, and significance tests are included. For the significance test, we generated surrogate BVs by randomly choosing the BV fields from original BVs so that the time dependence in the BV field is destroyed. These surrogate BV maps were regressed with the background Niño-3 index and the procedure repeated 100 times. Significance levels higher than 90% are shaded.

The result shows that the BV SST, surface height, and zonal wind stress all have a larger correlation before the mature stage of the ENSO events in the eastern Pacific. It also suggests coupled dynamics in the BV fields because of the increase of the ocean heat content and a warm SST anomaly in the eastern basin as well as the presence of westerly wind anomalies. The 2–3-month lead time in Figs. 7a,b coincides with the timing of the maximum of the BV growth rate in Fig. 2. This shows that the growing dynamic instability associated with the ENSO evolution in the NSIPP CGCM is dominant in the eastern Pacific. The sensitivity of the BV

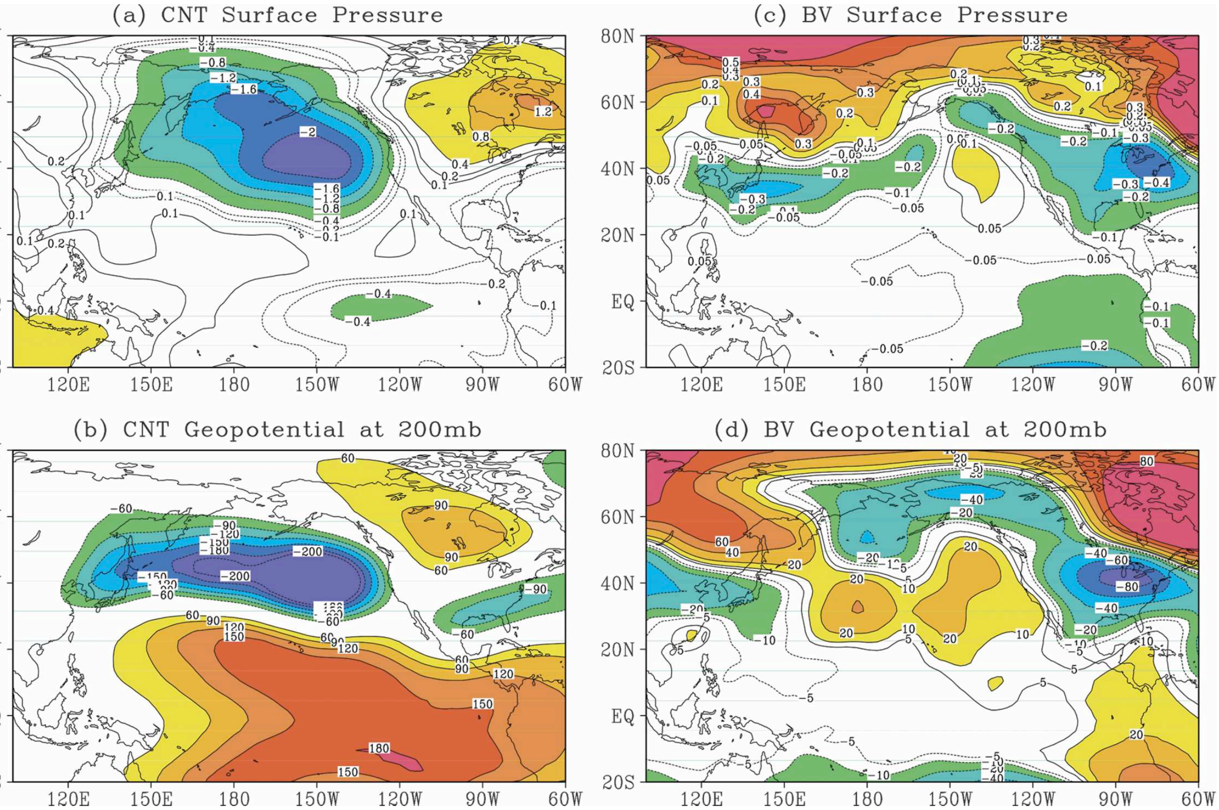

IG. 6. As in Fig. 3 except for atmospheric regression maps over the Pacific portion of the Northern Hemisphere: (a) background face pressure anomaly (hPa); (b) background geopotential anomaly at 200 hPa ($m^2 s^{-2}$); (c) BV surface pressure (hPa); and (d) BV potential at 200 hPa ($m^2 s^{-2}$).

potential use for ensemble forecasting, particularly the purpose of effectively perturbing the coupled NSO processes in the tropical Pacific.

Comparison of the NSIPP and the NCEP bred vectors

Similar breeding experiments were carried out with FS03 coupled model. The atmospheric component es the current version of medium-range forecast RF) global model with a spectral truncation of 62 ves (T62) in the horizontal (equivalent to nearly 200) and 64 vertical levels in sigma coordinate (Kanatsu et al. 1991; Saha et al. 2004). The ocean component is the Geophysical Fluid Dynamics Laboratory FDL) Modular Ocean Model V.3 (MOM3) with 40 ers in the vertical (Pacanowski and Griffies 1998). e zonal resolution is 1° and the meridional resolution ⅓° between 10°S and 10°N, gradually increasing ough the Tropics until it is fixed at 1° poleward of °S and 30°N.

Two independent breeding experiments were performed by choosing the last 4 yr from a 23-yr perfect period includes a warm event, which matures at model year 21, two years after starting the breeding run. The rescaling factor for NCEP bred perturbations is based on the SST norm computed over the whole tropical belt (10°S–10°N), not just in the tropical Pacific Niño-3 region like in the NSIPP BV. The perturbation size for the NCEP system was similar (0.1°C) and the rescaling period of one month was the same as in the breeding experiments performed with the NSIPP CGCM. Like the NSIPP coupled experiments, the two BV runs for the NCEP system were very similar despite having been started with different random perturbations so that their results are processed as a single 8-yr time series. Comparisons between the results from the NSIPP and the NCEP coupled system are now presented showing the extent to which bred vectors are sensitive to the coupled GCMs.[1]

We first compare the ENSO characteristics in the background runs of the two coupled GCMs. Figures

[1] Unfortunately, the experiments performed at NCEP were erased, so we have only a limited number of diagnostic compari-

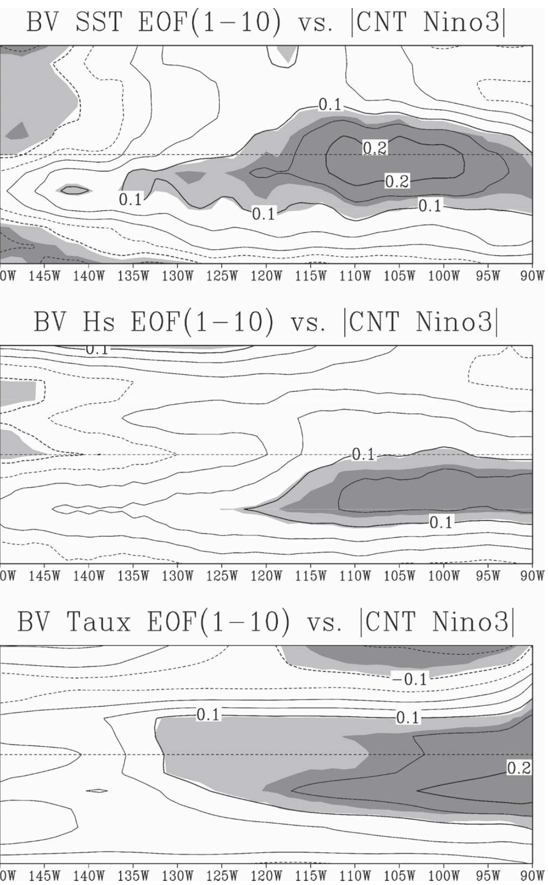

7. Lead/lag correlation maps along the equator for BV c fields, reconstructed with the first 10 EOF modes, against solute value of the background Niño-3 index: (a) SST (°C); face height (m); and (c) zonal wind stress (N m^{-2}). The dark) gray shading denotes the significance level higher 0% (95%).

re the background oceanic regression maps show- at the oceanic components from both CGCMs ssfully reproduce the fundamental features of . However, they also have differences reflecting ences of numerical schemes in the model dynam- different choices of physical parameterizations. meridional structure of warming and thickening e height (Figs. 8d,e) in the NCEP/CFS03 GCM in astern Pacific is wider than that of the NSIPP (Figs. 8a,b). In addition, the regressed surface t of NCEP/CFS03 shows the southern branch of oaling patterns off the equator extending farther ward instead of being meridionally limited as in SIPP case. This can also be seen in the SST and current patterns.

spite these differences in the background, the vectors from the two coupled systems have major ground ENSO. To compare BV structures, we show the leading EOFs of oceanic variables. Figures 9a–c are the first EOF mode of the BV SST and the first two modes for the BV thermocline from the NSIPP CGCM; Figs. 9d–f are the same modes using the BV from NCEP. Despite the fact that these are two different CGCMs with significantly different background evolution, there is a strong resemblance between the BV EOF modes. Both of the leading modes (EOF1) in NSIPP and NCEP bred vectors based on SST show an ENSO-associated warm feature in the tropical eastern Pacific farther east than in their respective background. Recalling that bred perturbations are rescaled in different regions (Niño-3 region for NSIPP and the complete tropical belt including three ocean basins for NCEP), the similarity observed in Figs. 9a and 9d indicates that the tropical Pacific dominates the growth of the BVs. However, reflecting the different mean structures and background ENSO variabilities from the two coupled systems, the NCEP BV EOF1 extends farther in space, covering the whole Niño-3 domain, while the NSIPP BV EOF1 is confined to east of 130°W and is limited in the meridional direction. The EOF1 modes representing ENSO variability explain 11% and 14% of the total variance of the growing SST perturbations in the NSIPP and NCEP models, respectively. Recall that the coupled growing perturbations include those due to a wide range of instabilities that appear in a coupled model. The fact that the leading EOF modes from BV fields in both coupled systems show a similar ENSO-like structure confirms our conjecture that the breeding method is capable of capturing the coupled instability even in the presence of other types of instabilities in the fully coupled GCM model. Moreover, this mode is robust and dominant since it is reproducible with different CGCMs and points out that the equatorial eastern Pacific is the most dynamically sensitive region for the growth of SST perturbations. Such a result indicates that the breeding method can help to identify the growing coupled instability related to the ENSO variability in a global coupled model.

Similar natural sensitivities in the eastern Pacific can also be found in the BV thermocline fields of both systems (Figs. 9b,c,e,f). For the background thermocline evolution (not shown), there are two dominant EOF modes related to the ENSO evolution: the leading one has a large variance in the eastern Pacific and the second one, representing an earlier transition, shows the anomalous deepening that starts from the subsurface of the western Pacific. We also examine the first two EOF modes for the BV thermocline. The result shows that

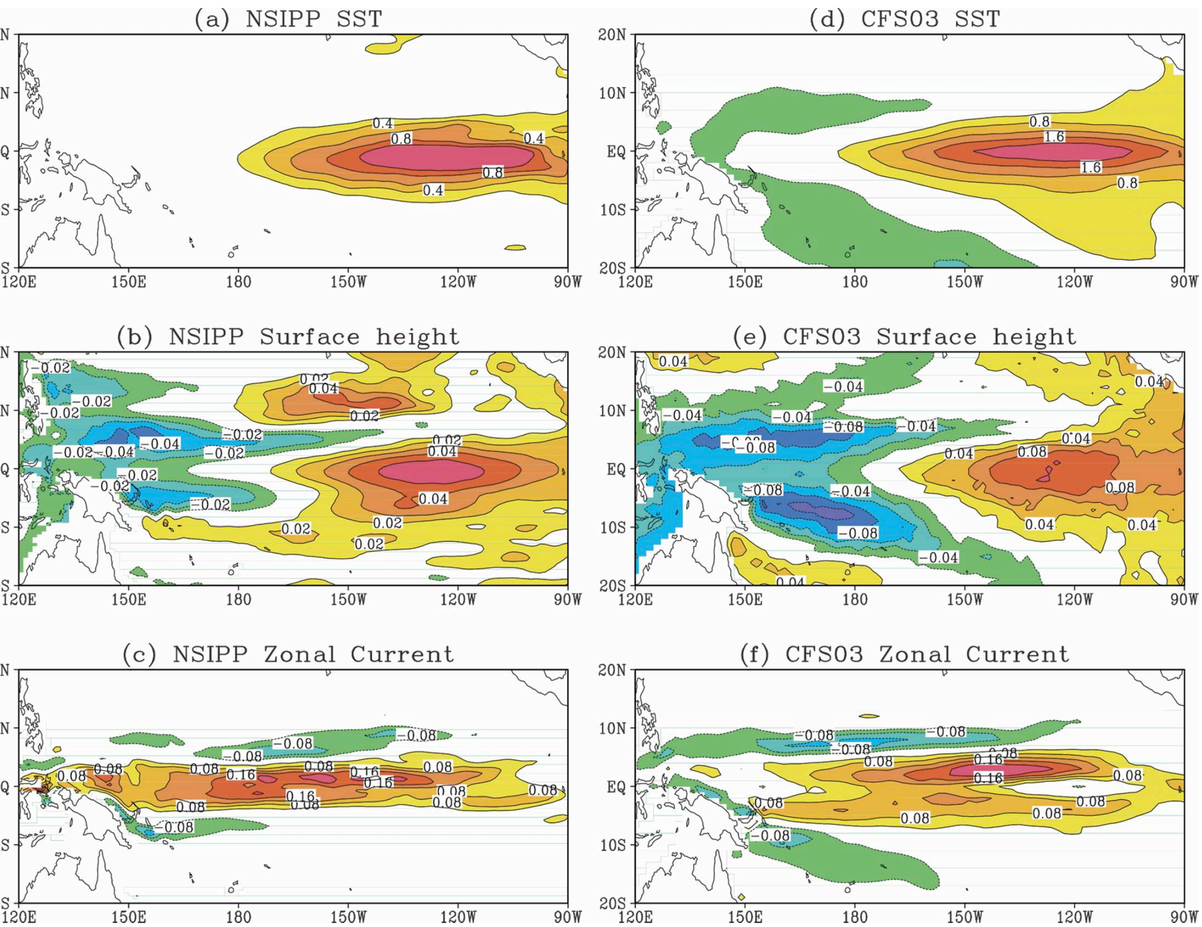

IG. 8. Background oceanic regression maps for two coupled GCMs in the tropical Pacific domain: (left) The NSIPP anomalies and ht) the NCEP/CFS03 anomalies. (a) NSIPP SST (°C); (b) NSIPP surface height (m); (c) NSIPP surface zonal current (m s^{-1}); (d) EP SST (°C); (e) NCEP surface height (m); and (f) NCEP surface zonal current (m s^{-1}). The regression maps of NSIPP (NCEP) ds are computed using the NSIPP (NCEP) Niño-3 index.

GCMs have a deepening feature along the equator d shoaling features off the equator in the eastern sin, except that the EOF1 from NCEP extends farer across the whole basin. In addition, both EOF2 odes have a dipole pattern along the equator and ablish a wave couplet off the equator in the western sin. The EOF2 emphasizes the role of the subsurface the western-central Pacific. Examining the BV thercline evolution off the equator, we found that the / thermocline also has an earlier westward propagan, like the background anomalies, and that the tim; of the westward propagation is linked with the ckground wind stress curl. These features in Fig. 9 d in the off-equator evolution suggest that the BV ermocline develops in a form of Kelvin/Rossby wave ckages, propagating the upwelling/downwelling sigs in the tropical region. It should be noted that the OF1 of the BV thermocline is closely related to the tween their corresponding leading principal components (not shown). These two modes represent the dominant growing coupled instability, which has also been obtained by the BV oceanic regression maps. The robustness of the results from two different coupled models supports our hypothesis that the leading EOFs of the bred vectors are associated with the background ENSO variability. The differences between the BVs indicate that bred vectors inherit the background characteristics associated with the model. For example, different vertical mixing schemes adopted in ocean models will have an impact on thermocline variations, particularly in the shallow mixed layer region.

Based on the regression maps against the BV Niño-3 index (not shown) in the tropical region, we can also infer that the coupling strengths are different in the two coupled GCMs. In both ocean components, a 1-m variation (deepening) in BV thermocline corresponds

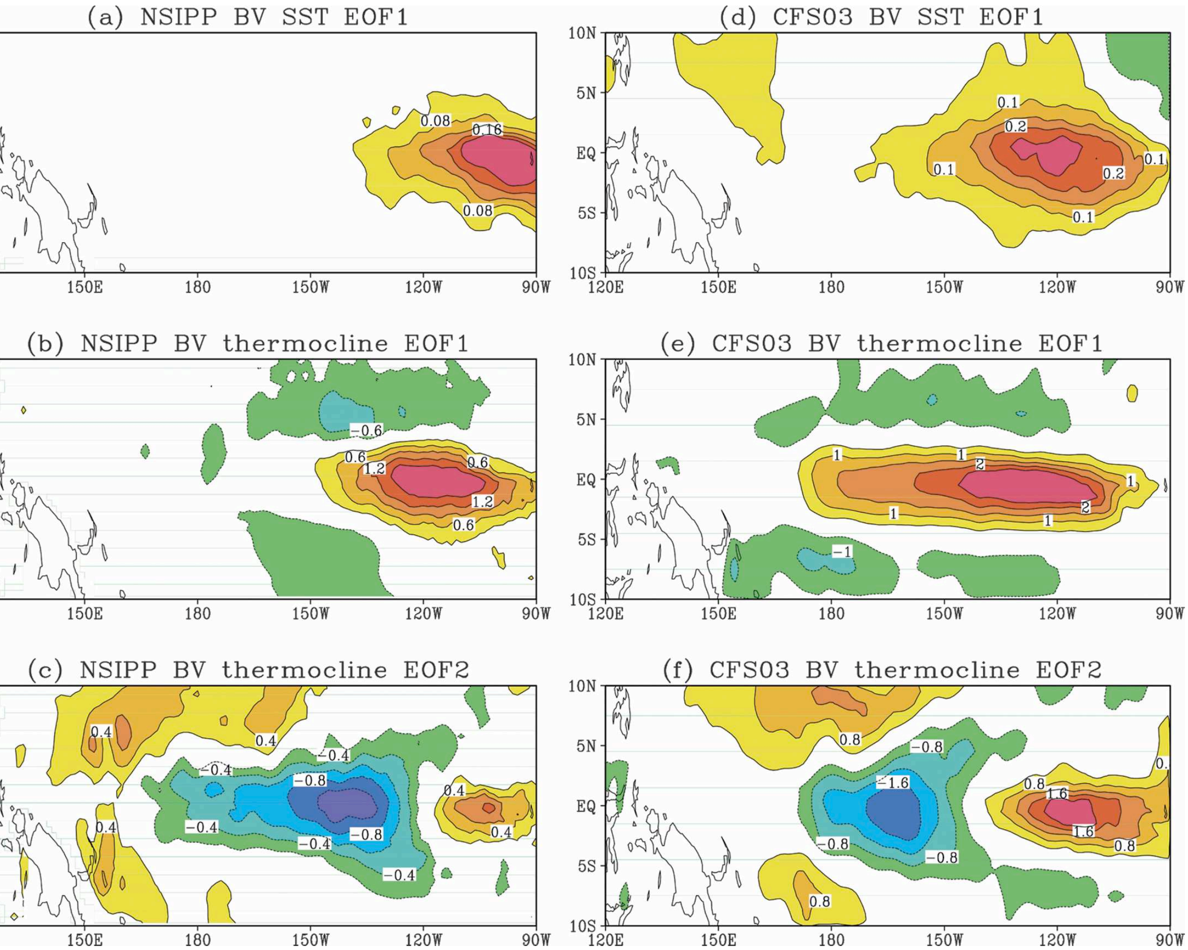

9. The leading EOFs of the BV SST and Z_{20} perturbations derived from the NSIPP and NCEP/CFS03 CGCMs: (a) EOF1 of BV SST; (b) EOF1 of NSIPP BV Z_{20}; (c) EOF2 of NSIPP BV Z_{20}; (d) EOF1 of NCEP BV SST; (e) EOF1 of NCEP BV Z_{20}; EOF2 of NCEP BV Z_{20}. The scale is arbitrary.

ing BV zonal wind stress shows a perturbation of m^{-2} from the NSIPP AGCM, and it prevails in entral basin. In contrast, the corresponding stress rbation is only 0.5 N m^{-2} in the NCEP case. In on, the regressed BV surface pressure and geo-tial height for the NCEP model are less organized Tropics than for the NSIPP coupled model. This s to suggest that tropical perturbations are more gly coupled in the NSIPP CGCM than in the P CGCM.

e similarity between the two systems can also be fied in the extratropical ENSO-associated tele-ection. Figures 10a,b are the regression maps of eopotential height at 500 hPa from the two ed models. Similar responses can be found from ortheastern Pacific to the North Atlantic despite fferent responses for other locations. These tele-cted regions are largely constrained by the varia-vectors in these locations suggests that the bred vector could be an "effective" ensemble ENSO perturbation in the sense that it projects the perturbation growth onto areas in the global atmosphere associated with ENSO variability.

Additional experiments with the NCEP/CFS03 CGCM have confirmed that the relationship between the BV growth rate and the phase of ENSO events remains similar with a rescaling period of 15-day rather than the one month used so far (M. Peña 2005, personal communication).

4. Summary and discussion

In this study, we demonstrated, for the first time, the feasibility of applying the breeding method to a global coupled ocean–atmosphere general circulation model to obtain ENSO coupled instabilities. The characteris-

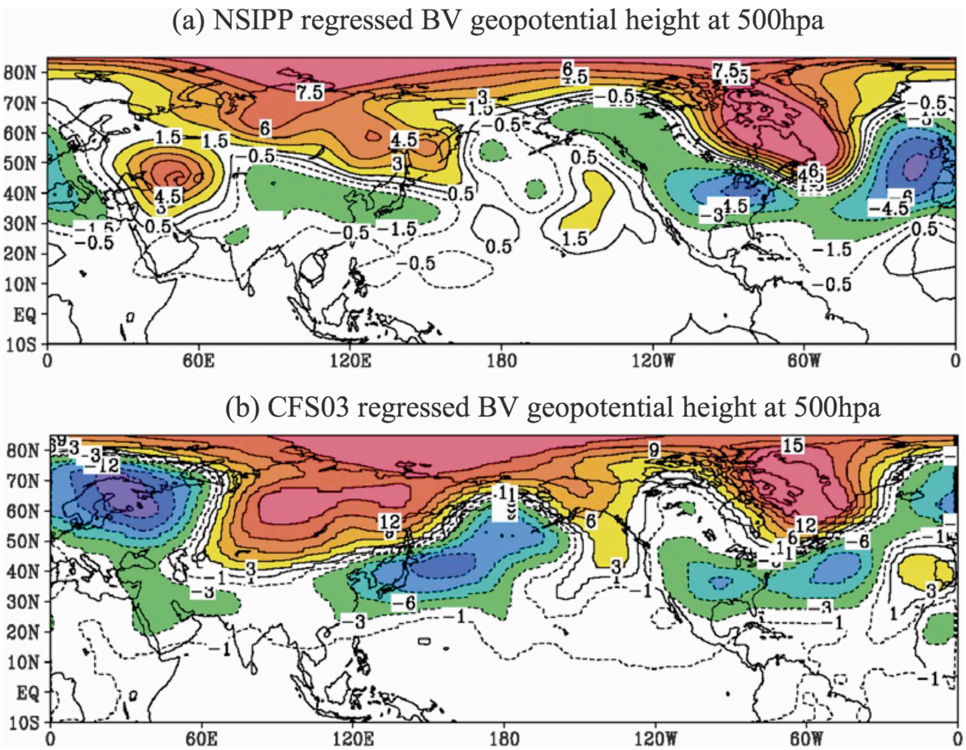

FIG. 10. Atmospheric regression maps in the Northern Hemisphere of BV sea level pressure (hPa) (a) for NSIPP and (b) for NCEP/CFS03. Both fields are computed against their own BV Niño-3 indices.

the NSIPP coupled model under a perfect model nario.

The results show that the breeding method can ob- n the growing coupled modes associated with ENSO riability and that the BV growth rate is sensitive to e background ENSO evolution, with the maximum ding the warm/cold events by three months. This d time in our results (compared with 6–12 months the ZC model) may seem to be too short for im- oving the current ensemble forecast system. How- er, we believe that this relatively short lead time is rtially due to the fact that the ENSO cycle in this long nulation is more biennial than 3–7 years. The biennial ne scale shortens the "growing season" of bred vec- s because of the relatively fast pace of the evolving ckground state. We would expect to obtain a longer d time from a BV growth rate derived from the IPP operational system since it will reflect the real eanic memory from the observations during initial- tion, although the shorter time lag may be also as- ciated with the presence of other weather and oce- c instabilities. We have explored this question with e current NSIPP operational system, which includes l ocean observations, and where we used as back- indicate that the lead time is lengthened by about 2 months.

One of the main tasks in our study has been to extract the physical growing mode from the total growth variability, separating the ENSO signal from noise associated with weather and other less relevant instabilities. We used regression BV maps to illustrate that the ENSO-associated features can be captured by the breeding method. For the oceanic fields, the variability mainly comes from the tropical eastern Pacific, where the background anomalies have large variance due to the mean structure of the thermocline. We also show that the atmospheric BV in the Tropics carries the coupled features reflecting the growing perturbations at the boundary due to the unstable air–sea interaction. Such structure exhibits a longitudinal Walker-like circulation along the equator. Evidence from the lead/lag correlation maps suggests that such growing perturbation is related to the background ENSO variability. In addition to the coupled characteristics shown in the tropical domain, the extratropical circulation anomalies associated with the coupled BV display a wave-train teleconnection pattern over the North Pacific and North America, areas known to be strongly telecone robustness of the coupled BV modes has been nstrated by comparing bred vectors derived from SIPP CGCM and NCEP/CFS03 CGCMs. The two ed GCMs can both represent the main features of NSO events, but differences exist in the detailed ure. Our results indicate that the coupled BV ure can be reproduced by the different CGCMs, ting very similar structure in their leading EOF s. In addition, the differences between the leading modes obtained from the two systems reflect that nherit the characteristics of the CGCMs. Strong blance between these two independent experi- s can be found in many fields, even in those atmo- ic teleconnected regions associated with back- d ENSO development. Our results suggest that lecting physically meaningful breeding param- one can use the breeding method to isolate the y varying, coupled instabilities from the fast- ng weather signals in a coupled GCM. The global ivities associated with the coupled instability ini- from the tropical Pacific can be retained even h the rescaling is simply done in the tropical Pa-

ng the same NSIPP CGCM, Kleeman et al. (2003) ated a climate-relevant leading singular vector by a tangent linear propagator derived from the sub- spanned by five dominant correlation EOF s of the background SST anomaly. In their work, focused on the SST perturbation, so we can only are the SST structure from the two methods. initial singular vector shows a large warming per- tion in the tropical Pacific with a maximum lo- in the central Pacific. Their final singular vector six months is very similar to our ocean regression (Fig. 3d) with a strong amplitude in the eastern c representing the mature state of ENSO. We do ave a warming feature in the northwest of the c off the equator that appears in the initial singu- ctor. In addition, there is no clear evidence show- at the singular vector is sensitive to the ENSO s even though the growth rates from both meth- how dependence on ENSO evolution. The simi- between the bred vector and the final singular r (but not the initial singular vector) is also char- stic of the results obtained with the ZC model et al. 2003; Xue et al. 1997b).

r results indicate that the coupled BVs could be in ensemble forecasting as initial perturbations ffectively project on the ENSO-related large-scale res. Therefore, the next stage of our research is to y these methods in the NSIPP operational sys- In particular, we plan to test whether ensemble more effective than current ensembles using uncoupled perturbations introduced into the atmosphere or the ocean model components.

Acknowledgments. We greatly appreciate many valuable discussions with Max. J. Suarez. We are very grateful to Sonya Kulkarni Miller for much technical support. We are grateful for the constructive comments and suggestions made by three anonymous reviewers that considerably improved the manuscript. The NSIPP component of this work has been supported by grants from the NASA Seasonal-to-Interannual Prediction Project (NASA-NAG-55825 and NASA-NAG-12418).

REFERENCES

Bacmeister, J., and M. J. Suarez, 2002: Wind stress simulations and the equatorial momentum budget in an AGCM. *J. Atmos. Sci.,* **59,** 3051–3073.

——, S. D. Schubert, M. Suarez, and P. J. Pegion, 2000: Atlas of seasonal means simulated by the NSIPP 1 atmospheric GCM. Technical Report Series on Global Modeling and Data Assimilation 104606, 17, 194 pp.

Battisti, D. S., 1988: The dynamics and thermodynamics of a warm event in a coupled tropical atmosphere–ocean model. *J. Atmos. Sci.,* **45,** 2889–2919.

Boffetta, G., A. Crisanti, F. Papatella, A. Provenzale, and A. Vulpiani, 1998: Slow and fast dynamics in coupled systems: A time series analysis view. *Physica D,* **116,** 301–312.

Cai, M., 1995: A simple model for the climatology and ENSO of equatorial Pacific ocean–atmosphere system. *Proc. 20th Annual Climate Diagnostics Workshop,* Seattle, WA, NOAA/CPC, 314–317.

——, 2003: Formation of the cold tongue and ENSO in the equatorial Pacific Basin. *J. Climate,* **16,** 144–155.

——, E. Kalnay, and Z. Toth, 2003: Bred vectors of the Zebiak–Cane model and their application to ENSO predictions. *J. Climate,* **16,** 40–55.

Cane, M. A., S. E. Zebiak, and S. C. Dolan, 1986: Experimental forecasts of El Niño. *Nature,* **321,** 827–832.

——, M. Münnich, and S. E. Zebiak, 1990: A study of self-excited oscillations of the tropical ocean–atmosphere system. Part I: Linear analysis. *J. Atmos. Sci.,* **47,** 1562–1577.

Chen, D., M. A. Cane, A. Kaplan, S. E. Zebiak, and D. Huang, 2004: Predictability of El Niño over the past 148 years. *Nature,* **428,** 733–736.

Chen, Y.-Q., D. S. Battisti, T. N. Palmer, J. Barsugli, and E. S. Sarachik, 1997: A study of the predictability of tropical Pacific SST in a coupled atmosphere–ocean model using singular vector analysis: The role of annual cycle and the ENSO cycle. *Mon. Wea. Rev.,* **125,** 831–845.

Contreras, R. F., 2002: Long-term observations of tropical instability waves. *J. Phys. Oceanogr.,* **32,** 2715–2722.

Dijkstra, H. A., and J. D. Neelin, 1999: Coupled process and the tropical climatology. Part III: Instabilities of the fully coupled climatology. *J. Climate,* **12,** 1630–1643.

Evans, E., N. Bhatti, J. Kinney, L. Pann, M. Peña, S.-C. Yang, E. Kalnay, and J. Hansen, 2004: RISE: Undergraduates find that regime changes in Lorenz's model are predictable. *Bull. Amer. Meteor. Soc.,* **85,** 520–524.

2000: How predictability depends on the nature of uncertainty in initial conditions in a coupled model of ENSO. *J. Climate,* **13,** 3298–3313.

F.-F., 1996: Tropical ocean–atmosphere interaction, the Pacific cold tongue, and the El Niño/Southern Oscillation. *Science,* **274,** 76–78.

–, 1997: An equatorial ocean recharge paradigm for ENSO. Part I: Conceptual model. *J. Atmos. Sci.,* **54,** 811–829.

namitsu, M., and Coauthors, 1991: Recent changes implemented into the global forecast system at NMC. *Wea. Forecasting,* **6,** 425–435.

eman, R., Y. Tang, and A. M. Moore, 2003: The calculation of climatically relevant singular vectors in the presence of weather noise as applied to the ENSO problem. *J. Atmos. Sci.,* **60,** 2856–2868.

ster, R. D., and M. J. Suarez, 1992: Modeling the land-surface boundary in climate models as a composite of independent vegetation stands. *J. Geophys. Res.,* **97,** 2697–2715.

if, M., and Coauthors, 1998: A review of predictability and prediction of ENSO. *J. Geophys. Res.,* **103,** 14 375–14 393.

ore, A. M., and R. Kleeman, 1996: The dynamics of error growth and predictability in a coupled model of ENSO. *Quart. J. Roy. Meteor. Soc.,* **122,** 1405–1446.

–, and ——, 1997: The singular vectors of a coupled ocean–atmosphere model of ENSO. Part II: Sensitivity studies and dynamical significance. *Quart. J. Roy. Meteor. Soc.,* **123,** 983–1006.

–, and ——, 1999a: Stochastic forcing of ENSO by the intraseasonal oscillation. *J. Climate,* **12,** 1199–1220.

–, and ——, 1999b: The non-normal nature of El Niño and intraseasonal variability. *J. Climate,* **12,** 2965–2982.

–, and ——, 2001: The differences between the optimal perturbations of coupled models of ENSO. *J. Climate,* **14,** 138–163.

anowski, R. C., and S. M. Griffies, 1998: MOM 3.0 manual. NOAA/Geophysical Fluid Dynamics Laboratory, Princeton, NJ.

ia, M., and E. Kalnay, 2004: Separating fast and slow modes in coupled chaotic systems. *Nonlinear Processes Geophys.,* **11,** 319–327.

land, C., and P. D. Sardeshmukh, 1995: The optimal growth of tropical sea surface temperature anomalies. *J. Climate,* **8,** 1999–2024.

necker, M., M. Suarez, D. Admec, R. Koster, S. Schubert, and J. Hansen, 2000: NASA Seasonal-to-Interannual Project (NSIPP) annual report for 2000. [Available online at http://nsipp.gsfc.nasa.gov/pubs/pubs_main.html.]

a, S., W. Wang, S. Nadiga, H.-L. Pan, and G. White, 2004: The new seasonal forecast model at NCEP. Preprints, *13th Conf. on Interactions of the Sea and Atmosphere,* Portland, ME, Amer. Meteor. Soc., CD-ROM, 3.8.

Schopf, P. S., and M. J. Suarez, 1988: Vacillations in a coupled ocean–atmosphere model. *J. Atmos. Sci.,* **45,** 549–566.

——, and A. Loughe, 1995: A reduced-gravity isopycnal ocean model: Hindcasts of El Niño. *Mon. Wea. Rev.,* **123,** 2839–2863.

Stockdale, T. N., D. L. T. Anderson, J. O. S. Alves, and M. A. Balmaseda, 1998: Global seasonal rainfall forecasts using a coupled ocean-atmosphere model. *Nature,* **392,** 370–373.

Suarez, M. J., and P. S. Schopf, 1988: A delayed action oscillator for ENSO. *J. Atmos. Sci.,* **45,** 3283–3287.

Thompson, C. J., 1998: Initial conditions for optimal growth in a coupled ocean–atmosphere model of ENSO. *J. Atmos. Sci.,* **55,** 537–557.

Toth, Z., and E. Kalnay, 1993: Ensemble forecasting at NMC: The generation of perturbations. *Bull. Amer. Meteor. Soc.,* **74,** 2317–2330.

——, and ——, 1996: Climate ensemble forecasts: How to create them? *Idojaras,* **100,** 43–52.

——, and ——, 1997: Ensemble forecast at NCEP and the breeding method. *Mon. Wea. Rev.,* **125,** 3297–3319.

Van der Vaart, P. C. F., H. A. Dijkstra, and F.-F. Jin, 2000: The Pacific cold tongue and the ENSO mode: A unified theory within the Zebiak–Cane model. *J. Atmos. Sci.,* **57,** 967–988.

Vialard, J., F. Vitart, M. A. Balmaseda, T. N. Stockdale, and D. L. Anderson, 2003: An ensemble generation method for seasonal forecasting with an ocean-atmosphere coupled model. ECMWF Tech. Memo. 417, 20 pp.

Vintzileos, A., M. M. Rienecker, M. J. Suarez, S. K. Miller, P. J. Pegion, and J. T. Bacmeister, 2003: Simulation of the El Niño-Interannual Prediction Project coupled general circulation model. *CLIVER Exchanges,* Vol. 8, No. 4, International CLIVAR Project Office, Southampton, United Kingdom, 25–27.

Xue, Y., M. A. Cane, S. E. Zebiak, and M. B. Blumenthal, 1994: On the prediction of ENSO: A study with a low order Markov model. *Tellus,* **46A,** 512–528.

——, ——, and ——, 1997a: Predictability of a coupled model of ENSO using singular vector analysis. Part I: Optimal growth in seasonal background and ENSO cycles. *Mon. Wea. Rev.,* **125,** 2043–2056.

——, ——, and ——, 1997b: Predictability of a coupled model of ENSO using singular vector analysis. Part II: Optimal growth and forecast skill. *Mon. Wea. Rev.,* **125,** 2057–2073.

Yang, S., K. Lau, and P. Schopf, 1999: Sensitivity of the tropical Pacific Ocean to precipitation induced freshwater flux. *Climate Dyn.,* **15,** 737–750.

Zebiak, S. E., and M. A. Cane, 1987: A model El Niño–Southern Oscillation. *Mon. Wea. Rev.,* **115,** 2262–2278.